



Full paper

Soft-contact cylindrical triboelectric-electromagnetic hybrid nanogenerator based on swing structure for ultra-low frequency water wave energy harvesting

Yawei Feng^{a,b}, Xi Liang^{a,b}, Jie An^{a,b}, Tao Jiang^{a,b,*}, Zhong Lin Wang^{a,b,c,*}

^a CAS Center for Excellence in Nanoscience, Beijing Key Laboratory of Micro-Nano Energy and Sensor, Beijing Institute of Nanoenergy and Nanosystems, Chinese Academy of Sciences, Beijing 100083, China

^b School of Nanoscience and Technology, University of Chinese Academy of Sciences, Beijing 100049, China

^c School of Materials Science and Engineering, Georgia Institute of Technology, Atlanta, GA 30332-0245, USA



ARTICLE INFO

Keywords:

Blue energy
Hybrid Nanogenerator
Triboelectric nanogenerators
Electromagnetic generator
Ultra-low frequency water waves
Swing structure

ABSTRACT

Ocean waves are promising green sources for energy exploitation, but harvesting such energy is quite challenging due to the apparent drawbacks of ultra-low vibration frequency and low efficiency. Here, a hybrid nanogenerator containing soft-contact cylindrical triboelectric nanogenerator and electromagnetic generator with swing structure was designed for ultra-low frequency wave energy converting. Brushes made of flexible rabbit hairs were introduced to separate stator-rotor pairs, with the function of charge pumping onto dielectric surface, which can reduce the operation resistance and improve the device durability. Based on the swing motion of rotor, over 60 current pulses can be generated within 15 s from either module by one external triggering, implying the output frequency multiplication and operation time extension. The optimized hybrid nanogenerator exhibits the best output response at 0.1 Hz of water wave agitation, delivering a peak power density of $10.16 \text{ W}\cdot\text{m}^{-3}$ and an average power density of $0.23 \text{ W}\cdot\text{m}^{-3}$. Furthermore, self-powered temperature mapping and wireless transmitting were successfully realized by a hybrid nanogenerator array to demonstrate its capability in collecting ultra-low frequency water wave energy. The distinctive structure and operation mechanism prompt the proposed hybrid nanogenerator to be a good candidate for large-scale blue energy harvesting.

1. Introduction

Rapid development of modern society puts forward increasing demands for energy sources [1], however, energy and environmental concerns have been raised in recent decades over the massive consumption of fossil-based fuels [2–4]. Due to the abundant and renewable features, ocean waves are regarded as potential energy sources for large-scale exploitations and applications [5–7]. What disappoints the engineers and researchers is the vibration characteristic of ultra-low frequency for ocean waves [7,8]. The ocean waves usually have a long period (can be over 10 s) and exhibit intermittent vibrations, leading to very low energy conversion efficiency. The development of generators suitable for ocean wave energy harvesting aims at multiplying the output frequency, extending the operation duration, and reducing the blank period, besides improving the instantaneous output performance.

Triboelectric nanogenerators (TENGs) have impressive applications in low-frequency mechanical energy harvesting [9–14], especially for the vibration frequency below several Hz [15–18]. Therefore, TENG is deemed to be a promising ocean wave energy converter [19–22], with the advantages of high-power density [23–26], light weight [20,27,28], low cost [29–31], and installation simplicity [32–37]. The operation principle of the most reported TENGs is based on the coupling effect of triboelectrification and electrostatic induction [38,39]. In order to improve the charge density on dielectric surface, sufficient contact is necessary for tribo-pairs to realize electronic cloud overlap for charge transfer (Wang transition in contact electrification) [40–42]. So it needs enough driving force to overcome the friction resistance and electrostatic attraction during operation [43]. But excessive contact friction will lead to material's wear and durability reduction [38]. To reduce the operation resistance and improve the durability are two prerequisites for

* Corresponding authors at: CAS Center for Excellence in Nanoscience, Beijing Key Laboratory of Micro-Nano Energy and Sensor, Beijing Institute of Nanoenergy and Nanosystems, Chinese Academy of Sciences, Beijing 100083, China.

E-mail addresses: jiangtao@binn.cas.cn (T. Jiang), zlwang@gatech.edu (Z.L. Wang).

<https://doi.org/10.1016/j.nanoen.2020.105625>

Received 28 September 2020; Received in revised form 12 November 2020; Accepted 17 November 2020

Available online 21 November 2020

2211-2855/© 2020 Elsevier Ltd. All rights reserved.

wide range applications of TENGs in ocean energy harvesting. In the previous work, pendulum-like spherical and swing-based cylindrical TENGs with air gaps for movement were fabricated for harvesting ultra-low frequency wave energy [44–46]. The special supporting structures enable the rotors to be suspended over the stator electrodes, which greatly extends the operation time and multiplies the output frequency. However, the power densities of the developed devices remain to be improved for better offshore applications.

In this work, a swing-structure-based hybrid nanogenerator made of soft-contact cylindrical TENG (SCC-TENG) and electromagnetic generator (EMG) was designed. Flexible rabbit hair brushes were introduced to separate the stator-rotor pair of the SCC-TENG. Through the friction between rabbit hair and fluorinated ethylene propylene (FEP) films, high density of charges ($> 20.3 \mu\text{C}/\text{m}^2$) were injected on the dielectric surfaces. Compared with traditional direct-contact or non-contact mode TENG, the introduction of flexible hair brushes in the SCC-TENG greatly reduced its operation resistance, enhanced the device durability, and solved the charge dissipation problem. An individual water wave triggering could generate more than 60 current pulses within 15 s for the optimized SCC-TENG. Under the water wave excitation at 0.1 Hz, the peak power density reached $2.71 \text{ W}\cdot\text{m}^{-3}$ and the average power density reached $0.16 \text{ W}\cdot\text{m}^{-3}$ at the matched resistance. By hybridizing with a modularized EMG, the output power was further improved. Finally, an array of hybridized nanogenerators was fabricated to demonstrate the applications in hydrological data monitoring and wireless transmission based on the ultra-low frequency water wave energy, indicating the potential toward large-scale blue energy for such proposed hybrid nanogenerator.

2. Results and discussion

2.1. Device structure and working principle

A swing-based hybrid nanogenerator consisting of a SCC-TENG and a modularized EMG was proposed for ocean wave energy harvesting, as

schematically shown in Fig. 1a and S1. The general device design was derived from our previous works [45,46]. The shell was printed by UV-curing resin or polylactic acid plastic, and 12 pieces of attached Cu electrodes were connected into two groups as terminals for energy outputs. The rotor is a stacked vane with a certain proportion of solid and hollow blades. Besides, thin FEP films were glued onto the external surface of rotor for electrostatic induction. A bearing component strung by a stainless shaft was used to support the stacked vane for swing motion. The tribo-pairs of most reported TENGs should be well contacted with each other in operation to ensure surface charges, while the FEP films and Cu electrodes in the designed SCC-TENG are separated both in function and structure. The external diameter of rotor is smaller than the inner diameter of the stator shell, and accordingly air gaps (less than 3 mm) are reserved between them (Fig. 1a-c and S1). To improve the charge density on the FEP surfaces, three tufts of dried rabbit hair were installed at the interval of 120° in the rectangular holes of the shell. Benefiting from the reserved gap and flexible hair brush, the driving force and friction resistance were largely reduced, accompanied by the multiplied working duration, output frequency and output power.

For further enhancing the output performance, an EMG module was hybridized into the above device. 3 Cu coils (Fig. 1d) were installed onto the external wall of the SCC-TENG shell, and 3 groups of neodymium magnets (Fig. 1e) were embedded into the bottom part of acrylic rotor. These magnets were magnetized along the thickness direction, and arranged in an arc configuration as shown in Fig. 1c. At static condition, each set of magnets corresponds to a Cu coil, meanwhile the barycenter of rotor is just below the bearing component, and the hair brushes (Fig. 1f) are located at the middle position of the adjacent blades (Fig. 1a).

The power generation of the fabricated SCC-TENG is based on the coupling effect of triboelectrification and electrostatic induction, however, the processes of triboelectrification and electrostatic induction are conducted by three components. As the fabricated rotor swings under an external excitation, negative charges will be accumulated on FEP film surfaces via rubbing with hair brushes (Fig. 2a and S2) to get saturated.

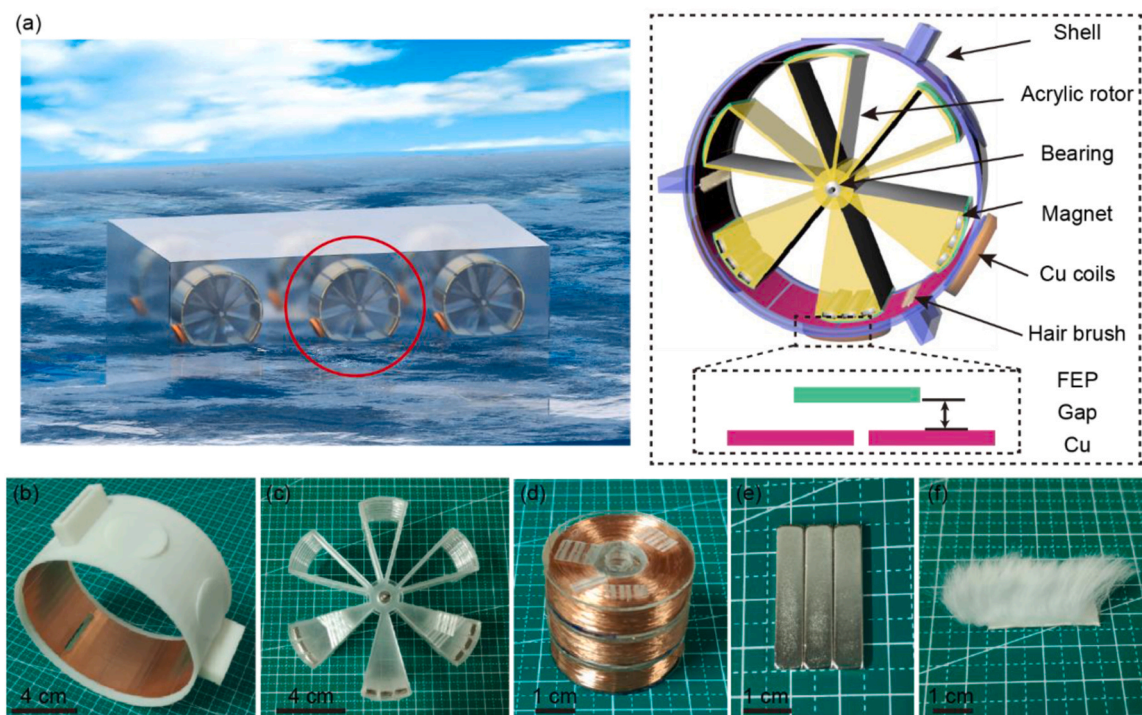


Fig. 1. Structural design and detailed components of the proposed hybrid nanogenerator. (a) Schematic illustrations of the hybrid nanogenerators and their application in ocean wave energy harvesting. The zoom-in illustration shows there is a gap between the FEP films and Cu electrodes. Photographs of (b) a printed shell with Cu electrodes, (c) a magnet-embedded rotor adhered with FEP films, (d) home-made Cu coils, (e) neodymium magnets, and (f) a rabbit hair brush.

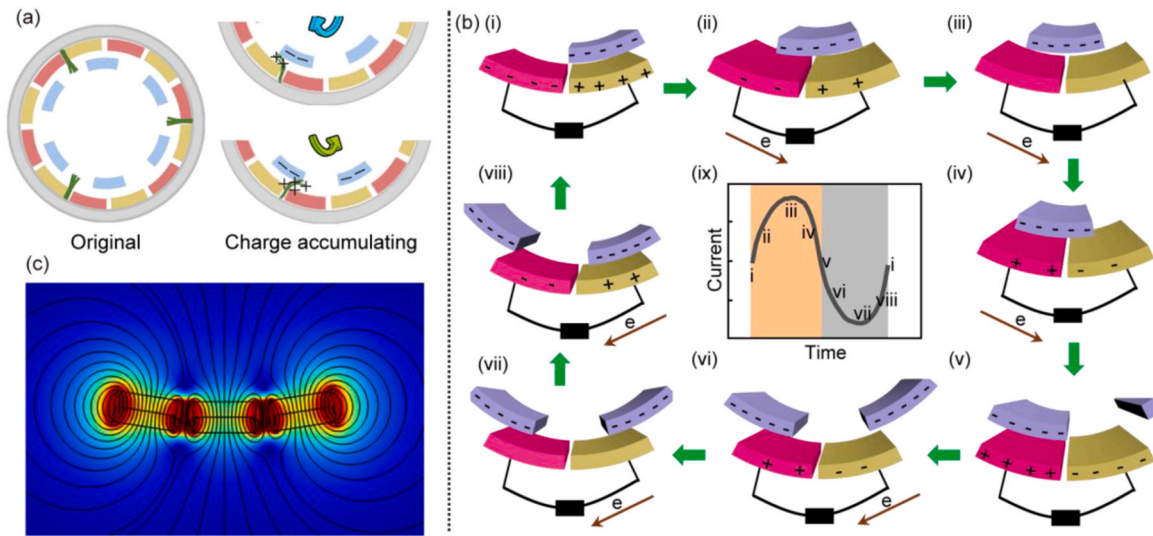


Fig. 2. Working principle of the hybrid nanogenerator. Schematic operation principle of the SCC-TENG for (a) triboelectrification and (b) electrostatic induction. (c) Simulated magnetic lines of flux for one group of magnets by COMSOL.

Fig. 2b shows the schematic principle for the power generation by presenting a part of the SCC-TENG structure. At state (i), opposite net charges are generated on different electrodes by electrostatic induction of the negatively charged FEP film, where the charge density on either

electrode is lower than that on FEP films due to the existing gap. Once an external excitation is applied, the rotor will naturally swing leftward (Fig. 2b) or rightward (not shown). During the leftward swing motion [states (i)-(v)], free electrons are driven to flow from the left electrode to

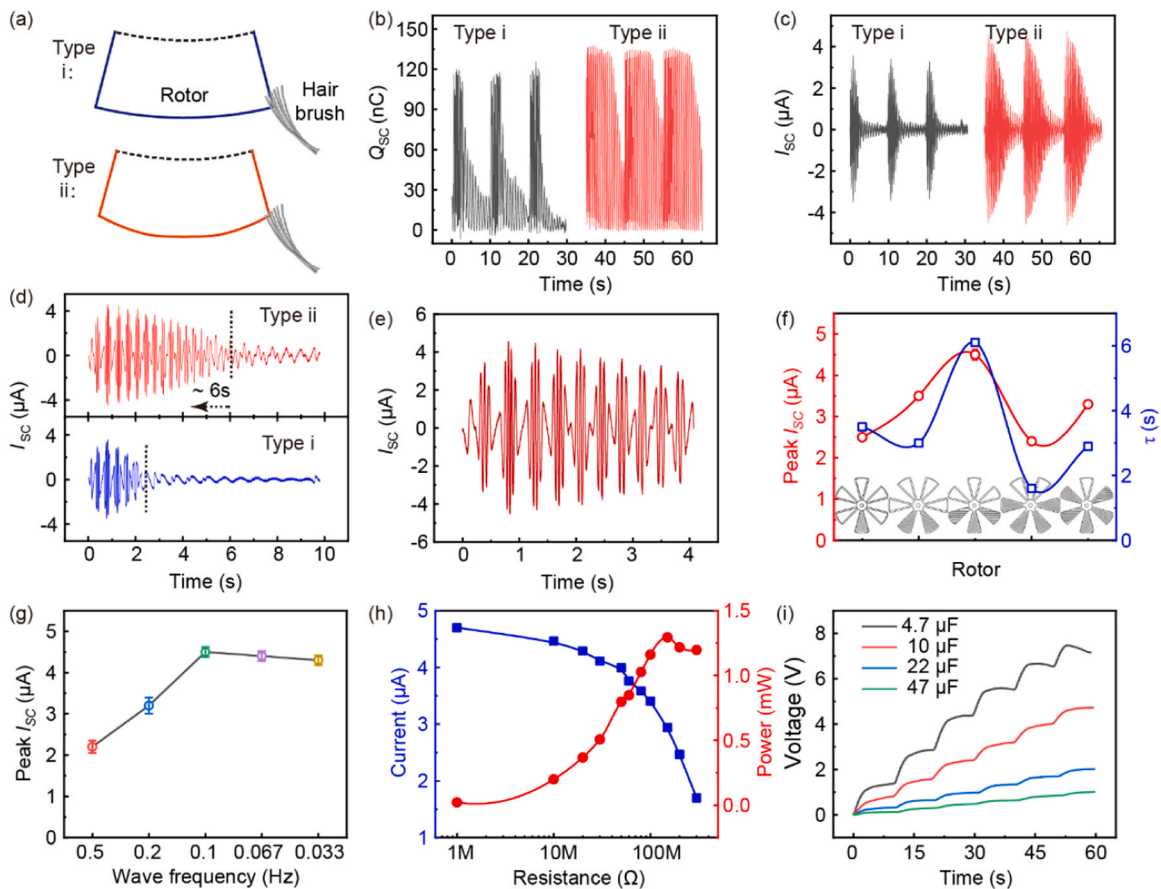


Fig. 3. Performance optimization of the SCC-TENG in water. (a) Schematic illustration for the two types of blades. Waveform comparison of (b) Q_{sc} , (c) I_{sc} and (d) I_{sc} under one excitation for the two types of blades triggered by the water waves of 0.1 Hz. (e) The enlarged view of I_{sc} waveform within the first 4 s for the SCC-TENG with a Type ii blade. (f) Extracted peak I_{sc} and τ values for the devices fabricated by rotors with various shapes. (g) Peak I_{sc} generated from the optimized device under different water wave frequencies. (h) Instantaneous peak current and power-resistance relationships of the optimized SCC-TENG and (i) its performance for charging different capacitors.

the right one through the external circuit, generating a current from the right electrode to the left one. After the rotor swings to pass a whole electrode [states (v)-(viii)] or swings rightward, the electrons flow backward to the left electrode, generating a reversed current pulse. By swinging over two Cu electrodes, a whole cycle of electron flow is formed as shown in Fig. 2b(ix).

The well-understood generation mechanism of EMG is based on electromagnetic induction [47,48]. The simulated magnetic flux lines (Fig. 2c) describe the distribution of magnetic field, while the magnets were magnetized along the thickness direction. The voltage from the EMG either in open-circuit state or loaded with a resistance is several orders of magnitude smaller than that from the SCC-TEG. Hence the coils were connected in series in the same winding direction for the EMG voltage superposition. The installation configuration of magnets and coils enables the coils to cut the magnetic flux lines to a maximum degree, and thus intense current is induced in Cu coils as the rotor swings. Because of the symmetric and centrosymmetric installation layout of EMG and SCC-TEG, the waveforms of a typical output parameter from both modules with distinct generation mechanisms are the same, regardless of clockwise or counterclockwise swinging.

2.2. SCC-TEG optimization and its performance

The swing motion of rotor is mainly hindered by the resistance from hair brushes, as well as the one from bearing components, air, and electrostatic attraction between rotor and hair brushes. Due to the dominant resistance from the friction with the hair brushes, the rotor profile was first considered for the performance optimization. Two types of blades with different cutting profiles were prepared. One is a common fan-shaped blade (Type i), while the other has smooth edges in the chamfer regions (Type ii), as shown in Fig. 3a. To contact with FEP films, the installed hair brushes are protruded for several millimeters. Contributed to the chamfer edges for Type ii, the FEP film surface can be well charged and the operation resistance is largely reduced. Hence, more transferred charges (Q_{SC} of 135 nC, Fig. 3b) and higher peak short-circuit current (I_{SC} of 4.57 μ A, Fig. 3c) were achieved at a water wave excitation frequency of 0.1 Hz. By contrast, the SCC-TEG with the rotor of Type i exhibited less Q_{SC} (118 nC) and lower I_{SC} (3.39 μ A) values. The enlarged views for the I_{SC} waveform of both SCC-TEGs under one excitation are presented for comparison in Fig. 3d. The time that the rotor swings through at least one electrode area was defined as τ . The τ value for the SCC-TEG of Type ii is 6.1s, but 2.4s for Type i, which indicates the superior operation condition of Type ii device and faster performance decay of Type i device. A video recording the swing motion triggered by linear motor (Video S1) can visualize this working condition. The sharp patterns and numerous current pulses (Fig. 3e) imply the fast electron transfer under electrostatic induction. Under water excitation at the frequency of 0.1 Hz, about 60 current pulses are created, suggesting the multiplication ability for output frequency.

Supplementary material related to this article can be found online at [doi:10.1016/j.nanoen.2020.105625](https://doi.org/10.1016/j.nanoen.2020.105625).

Inappropriate barycenter offset by excessive or insufficient rotor mass would lead to the inferior performance. The rotor shape, as an important factor influencing the barycenter offset in swing motion, was also optimized. Five kinds of rotors with different ratios of solid to hollow blades, as illustrated in Fig. 3f, were prepared by laser cutting. The fabricated device using equal number of solid and hollow blades possesses the best values of I_{SC} and τ . In addition, its open-circuit voltage (V_{OC}) is estimated to be about 640 V (Fig. S3). Hence such SCC-TEG with 3 solid and 3 hollow blades was selected for the subsequent hybridization with EMG module. Besides, the effect of the water wave triggering frequency on the output performance was also investigated, indicating that 0.1 Hz is the optimum frequency for the SCC-TEG to get the highest peak I_{SC} (Fig. 3g). Higher frequency would lead to insufficient swing amplitude, while lower frequency would cause redundant hiatus along with the slight decrease in instantaneous power. The

decreased wave height could also seriously affect the output performance by attenuated driving force (Fig. S4). It seems that the employed magnet number rarely affects the SCC-TEG performance (Fig. S5), resulting from the decoupling of electromagnetic induction from EMG and TENG, as well as the inapparent displacement of rotor barycenter. Additionally, the peak I_{SC} shows no noticeable decrease after rectification (DB107 rectifier bridge) (Fig. S6).

Under the optimal external environment (triggering frequency of 0.1 Hz, wave height of 10 cm), an instantaneous peak power of 1.29 mW (Fig. 3h) is achieved at the matched resistance of 150 $\text{M}\Omega$, corresponding to a peak power density of $2.71 \text{ W}\cdot\text{m}^{-3}$ and an average power density of $0.16 \text{ W}\cdot\text{m}^{-3}$. The internal conversion efficiency (Fig. S7) is evaluated to be over 3.7%. Such SCC-TEG can charge 4.7, 10, 22, 47 μF capacitors to 7.2, 4.7, 2.0, 1.0 V within 60 s in the water waves at 0.1 Hz and 10 cm (Fig. 3i). Also the charging voltage can be elevated by increasing the wave frequency (Fig. S8). Besides, contributed to the friction with flexible brushes, not direct contact with stator electrodes, no obvious performance attenuation (Fig. S9a) and material abrasion (Fig. S9b-c) were observed after long-term cycles, verifying the improving strategy for the device durability and stability.

2.3. EMG performance

The output paths of the fabricated EMG and SCC-TEG are separated, although the modularized EMG is closely attached to the SCC-TEG shell. There is no coupling effect between them for the mismatched induction, and thus little interference in performance with each other (Fig. S5). The operation of EMG module is also based on the swing structure, and the weights of magnets and the acrylic carved out for installing the magnets are approximate, so the EMG optimization is accompanied with the SCC-TEG optimization. The ultimate EMG containing three magnet-coil pairs can fully utilize the device configuration. Due to the principle of electromagnetic induction, the current from EMG is several orders of magnitude larger than that from TENG, but the voltage is contrary. As shown in Fig. 4a and S10, the peak I_{SC} and V_{OC} generated by the EMG in the water waves with the frequency of 0.1 Hz and the height of 10 cm are 11.9 mA and 2.9 V, respectively. Their waveforms of current and voltage are similar to those of the SCC-TEG, and the impacts of the triggering wave frequency (Fig. 4b) and height (Fig. S11) are also similar. The influence of the magnet-coil pair number on the EMG performance was also studied, indicating that the peak V_{OC} and I_{SC} can be raised by increasing the magnet group number (Fig. 4c).

Unlike the remained current intensity from the SCC-TEG after rectification, the rectified current from the EMG remarkably reduces (Fig. 4d). Its peak intensity drops to 57.2% of the original value due to the diodes' threshold voltage. After rectification, the EMG produces an instantaneous peak power of 3.5 mW at the matched resistance of 300 Ω (Fig. 4e) under the water wave conditions of 0.1 Hz and 10 cm, corresponding to a peak power density of $7.45 \text{ W}\cdot\text{m}^{-3}$ and an average power density of $0.07 \text{ W}\cdot\text{m}^{-3}$ (Fig. S12). This peak density is larger than that of the SCC-TEG at the same conditions for its higher current density. However, the average power density is lower than that of the SCC-TEG, caused by the decreased pulse number, narrowed peak width (Fig. S12a), and redundant hiatus (Fig. S12b-c). Such EMG module can charge a capacitor at a faster rate than the SCC-TEG. But due to the lower V_{OC} of EMG module, the voltage on the capacitor quickly reaches a limiting value. For example, under the water wave triggering for three times at 0.1 Hz and 10 cm, the capacitors of 200, 470 and 1000 μF can be charged to the limiting voltage ($\sim 1.3 \text{ V}$) for the EMG module.

2.4. Hybrid array device and application demonstration

By connecting the output terminals of the TENG and EMG in parallel, a hybrid nanogenerator was fabricated. The performance of the developed triboelectric-electromagnetic hybrid nanogenerator is the

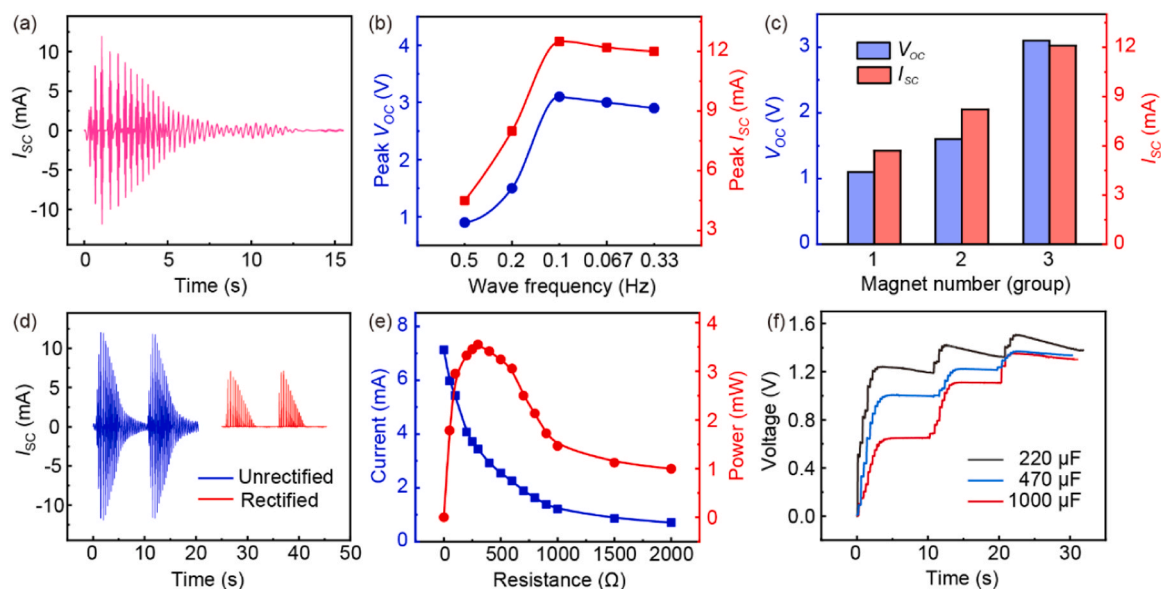


Fig. 4. Output performance of the EMG in water. (a) The waveform of I_{sc} under one water wave triggering. (b) Peak V_{oc} and I_{sc} with respect to the wave frequency under the water wave triggering. (c) Performance variation of the EMG as a function of the number of magnet groups. (d) Comparison of the I_{sc} waveform before and after rectification. (e) Instantaneous peak current and power-resistance relationship profiles for the EMG after the rectification and (f) charging performance of the EMG for different capacitors.

mathematical summation of individual generator performance under the same excitation conditions, because there is no mutual interference in performance measurement. As a result, the developed hybrid device achieves a peak power of 4.8 mW at the optimum water wave conditions and loading resistances, which corresponds to a peak power density of $10.16 \text{ W}\cdot\text{m}^{-3}$, an average power density of $0.23 \text{ W}\cdot\text{m}^{-3}$, and an internal harvesting efficiency of 5.3%. Such peak and average power densities are several- to tens-fold higher than the previous reported device for ultra-low frequency water wave harvesting [44,46]. Due to the larger V_{oc} of the SCC-TENG module, 60 green LED bulbs (Fig. S13a and Video S2) can be continuously powered for luminescence under the water wave excitation of 0.1 Hz. Nevertheless, the lower voltage from the EMG module is insufficient to light the LED bulbs with a rated voltage of 3 V, in spite of the higher current. Combining the individual advantages of both modules, that is higher V_{oc} of the SCC-TENG and larger I_{sc} of the EMG, a specific capacitor can be charged faster or to a higher voltage compared with either module (Fig. S13b). As an application demonstration (Fig. S13c-d), the hybrid nanogenerator can continuously power a thermometer for temperature monitoring by charging a capacitor.

Supplementary material related to this article can be found online at [doi:10.1016/j.nanoen.2020.105625](https://doi.org/10.1016/j.nanoen.2020.105625).

By arraying the developed hybrid nanogenerators, it is promising for particular applications such as water wave energy harvesting, even toward the explication of blue energy conversion. A photograph of the array with 6 units placed into an acrylic box and the brief arraying process are shown in Fig. 5a-b. Only one hybrid nanogenerator is installed in the array, and the rest are SCC-TENGs. One reason is that the magnet-coil pairs are too heavy to be excited by the simulated waves. In addition, due to the apparent voltage decrease, the EMG modules are failed in power manage after rectification, no matter in series or parallel connection. Thus, only one hybrid nanogenerator in the array is preserved. The paralleled SCC-TENGs give increasing peak I_{sc} value with an approximately linear correlation versus the increasing unit number (Fig. 5c). After paralleling six SCC-TENG units, the I_{sc} increases to 23.1 μA under the wave agitation (0.1 Hz, 10 cm).

Two demonstrations were performed to illustrate the applications of hybrid nanogenerators by water wave energy harvesting. For both demonstrations, capacitors were applied to store the pulsed energy and output stable energy. The optimal water waves with the conditions of

0.1 Hz and 10 cm were applied to reveal the ability of the hybrid array device in ultra-low frequency wave energy harvesting. In the first application (Fig. 5d-e, Video S3), a self-powered hydrological data mapping system was constructed by combining a thermometer array and the hybrid nanogenerator array. A 330 μF capacitor was charged to 3.0 V within 120 s by the hybrid array. The thermometer array is set to have an on-off cycle of 20 s, and the working time is 5 s in one cycle. Thus, the temperature data in different water areas can be collected intermittently. During the temperature mapping process, the voltage on the capacitor is maintained at 2.8–3.0 V (Fig. 5e), which ensures the stable operation of the thermometers.

Supplementary material related to this article can be found online at [doi:10.1016/j.nanoen.2020.105625](https://doi.org/10.1016/j.nanoen.2020.105625).

For the next application, we constructed a self-powered wireless transmitting system. A wireless transmitter (EV1527) which can send a signal to the receiver to turn on an alarm is shown in Fig. 5f-g and Video S4. The transmitting distance can be tens to hundreds of meters away, which is dependent of the driving power. In our demonstration, a distance of only 1.2 m between the transmitter and the receiver is shown due to the space limitation. After the capacitor of 1000 μF was charged to about 4.1 V within 540 s, the switch was closed to power the transmitter for sending signals, and then the alarm was turned on to send out sound and light. The self-powered temperature mapping and wireless transmitting have successfully demonstrated the applications of proposed hybrid nanogenerators by water wave energy harvesting (Fig. 5h), which are conceived to expand for ocean environment monitoring, modern fishery culture, and even blue energy exploitation.

Supplementary material related to this article can be found online at [doi:10.1016/j.nanoen.2020.105625](https://doi.org/10.1016/j.nanoen.2020.105625).

3. Conclusion

In summary, a swing-structure-based hybrid nanogenerator with SCC-TENG and EMG has been designed for harvesting ultra-low frequency water wave energy. The installed flexible hair brushes not only pump high density of charges onto FEP surface, but also separate dielectric FEP rotor and Cu electrodes of the SCC-TENG for reducing operation resistance and improving durability. The optimized hybrid device can continuously operate for about 15 s under one external

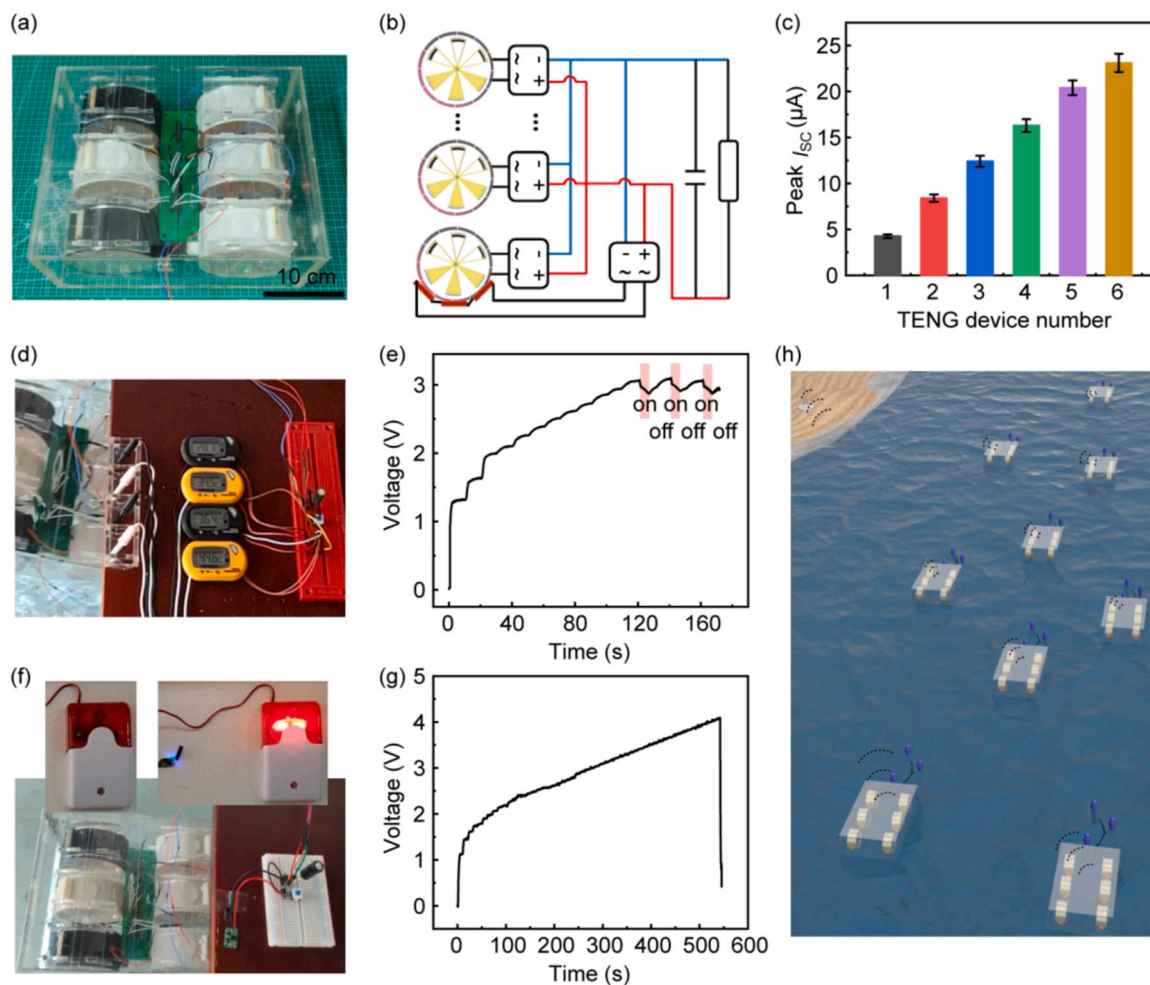


Fig. 5. Application demonstrations of the hybrid array in hydrological monitoring by water wave energy harvesting. (a) Photograph of the array device with 6 units. (b) Schematic circuit diagram of the arrayed nanogenerators. Five of them are SCC-TENGs, and the other is a hybrid unit. (c) Extracted peak I_{sc} of the SCC-TENG array as a function of the parallel unit number. (d-e) Powering a thermometer array by charging a 330 μF capacitor, and (f-g) powering a wireless transmitter by charging a 1000 μF capacitor. (h) A blueprint exhibiting the self-powered applications of proposed hybrid nanogenerators in hydrological monitoring and data transmission by large-scale blue energy harvesting. (For interpretation of the references to colour in this figure legend, the reader is referred to the web version of this article.)

excitation. Besides the prolonged output duration, the grid electrode and reasonable magnet-coil installation are conducive to more than 60 current pulses from each module by one triggering, realizing amplification of output frequency. When agitated by the water waves at 0.1 Hz, the hybrid nanogenerator exhibits the best output response, producing an instantaneous peak power of 4.8 mW, which corresponds to a peak power density of $10.16 \text{ W}\cdot\text{m}^{-3}$ and an average power density of $0.23 \text{ W}\cdot\text{m}^{-3}$. That indicates the excellent harvesting capacity of ultra-low frequency water waves for such nanogenerator. Finally, the self-powered temperature mapping and wireless transmitting have been successfully demonstrated by an array consisting of hybrid nanogenerator and parallel SCC-TENG units in ultra-low frequency water waves. The hybrid nanogenerators are conceived to have potential applications in ocean current monitoring, modern fishery culture, and even large-scale blue energy development by hybrid nanogenerator networks.

4. Experimental methods

4.1. Fabrication of the SCC-TENG

The shell of SCC-TENG was printed by UV-curing resin (white) or polylactic acid (black). The inner diameter of shell is 100 mm, and the wall thickness is 2 mm. Twelve Cu electrodes with the same size of

$25 \text{ mm} \times 45 \text{ mm} \times 30 \mu\text{m}$ were adhered to the inner side of the cylindrical shell, and were organized to two groups for energy outputs. Three rectangular holes ($30 \text{ mm} \times 4 \text{ mm}$) were reserved at the interval of 120° for the introduction of rabbit hair brushes. Rabbit fur was cut into pieces with the size of $4 \text{ mm} \times 30 \text{ mm}$. The hair length is about 20 mm, thus the reserved holes on the shell were protruded for 15 mm to fix the hair. For the rotor, acrylic plates were tailored by laser cutting into the designed shapes (external diameter of 97 mm). Several blades with bearings (external diameter of 6 mm, internal diameter of 2 mm, thickness of 2.5 mm) were stacked to 44 mm in total thickness, and then strung by a steel wire (φ : 2 mm) for rotor fabrication. FEP films ($30 \mu\text{m}$ in thickness) were adhered onto the external surface of the rotor as the dielectric layers. After all components were dried in a vacuum oven at 40°C for at least 4 h, the SCC-TENG was sealed by circular plates for the performance measurements.

4.2. Fabrication of the hybrid nanogenerator

For the fabrication of hybrid nanogenerator, three home-made Cu coils (φ : 0.2 mm, external diameter of 35 mm, internal diameter of 15 mm, thickness of 10 mm) were attached onto the shell surface, and the coils were connected in series. Besides, the bottom part of rotor was embedded with 3 groups of bar neodymium magnets

(30 mm × 6 mm × 3 mm, magnetized along the thickness direction, 2490 Gs) before being sealed. Each group of magnets consists of 3 units, which are all arranged in an arc shape in the same magnetization direction to ensure multiplicative performance.

4.3. Characterizations and measurements

A Keithley 6514 system electrometer was employed for measurements of open-circuit voltage (V_{OC}), short-circuit transferred charge (Q_{SC}) and current (I). The distribution of magnetic lines of flux for one group of magnets was simulated by COMSOL Multiphysics 5.4. The characterizations in water waves were carried out in a water tank. A push plate controlled by a programmable digital controller was used for generating the water waves. Porous cushions were used as wave absorber for the elimination of rebound waves.

CRedit authorship contribution statement

Yawei Feng: Conceptualization, Methodology, Visualization, Data curation, Writing - original draft. **Xi Liang:** Methodology, Validation, Resources, Writing - review & editing. **Jie An:** Resources, Writing - review & editing. **Tao Jiang:** Conceptualization, Methodology, Supervision, Writing - review & editing. **Zhong Lin Wang:** Conceptualization, Methodology, Supervision, Writing - review & editing.

Declaration of Competing Interest

The authors declare that they have no known competing financial interests or personal relationships that could have appeared to influence the work reported in this paper.

Acknowledgments

Supports from the National Key R & D Project from Minister of Science and Technology (2016YFA0202704), National Natural Science Foundation of China (Grant Nos. 51432005, 51702018, and 51561145021) and Youth Innovation Promotion Association, CAS, are appreciated. The authors also thank Jiajia Shao and Pengfei Chen in the Beijing Institute of Nanoenergy and Nanosystems for device fabrications and measurements.

Appendix A. Supporting information

Supplementary data associated with this article can be found in the online version at [doi:10.1016/j.nanoen.2020.105625](https://doi.org/10.1016/j.nanoen.2020.105625).

References

- [1] Z.L. Wang, Entropy theory of distributed energy for internet of things, *Nano Energy* 58 (2019) 669–672.
- [2] S.D. Musa, T. Zhonghua, A.O. Ibrahim, M. Habib, China's energy status: a critical look at fossils and renewable options, *Renew. Sustain. Energy Rev.* 81 (2018) 2281–2290.
- [3] A. Shahsavari, M. Akbari, Potential of solar energy in developing countries for reducing energy-related emissions, *Renew. Sustain. Energy Rev.* 90 (2018) 275–291.
- [4] Y. Kuang, Y. Zhang, B. Zhou, C. Li, Y. Cao, L. Li, L. Zeng, A review of renewable energy utilization in islands, *Renew. Sustain. Energy Rev.* 59 (2016) 504–513.
- [5] J. Scruggs, P. Jacob, Harvesting ocean wave energy, *Science* 323 (2009) 1176–1178.
- [6] J. Tollefson, Power from the oceans: blue energy, *Nature* 508 (2014) 302–304.
- [7] A. Ilyas, S.A.R. Kashif, M.A. Saqib, M.M. Asad, Wave electrical energy systems: implementation, challenges and environmental issues, *Renew. Sustain. Energy Rev.* 40 (2014) 260–268.
- [8] C. Garrett, W. Munk, Internal waves in the ocean, *Annu. Rev. Fluid Mech.* 11 (1979) 339–369.
- [9] F.-R. Fan, Z.-Q. Tian, Z. Lin Wang, Flexible triboelectric generator, *Nano Energy* 1 (2012) 328–334.
- [10] C. Wu, A.C. Wang, W. Ding, H. Guo, Z.L. Wang, Triboelectric nanogenerator: a foundation of the energy for the new era, *Adv. Energy Mater.* 9 (2019), 1802906.
- [11] T. Cheng, Q. Gao, Z.L. Wang, The current development and future outlook of triboelectric nanogenerators: a survey of literature, *Adv. Mater. Technol.* 4 (2019), 1800588.
- [12] J. Nie, X. Chen, Z.L. Wang, Electrically responsive materials and devices directly driven by the high voltage of triboelectric nanogenerators, *Adv. Funct. Mater.* 28 (2018), 1806351.
- [13] X. Peng, K. Dong, C. Ye, Y. Jiang, S. Zhai, R. Cheng, D. Liu, X. Gao, J. Wang, Z. L. Wang, A breathable, biodegradable, antibacterial, and self-powered electronic skin based on all-nanofiber triboelectric nanogenerators, *Sci. Adv.* 6 (2020), eaba9624.
- [14] Y. Feng, K. Han, T. Jiang, Z. Bian, X. Liang, X. Cao, H. Li, Z.L. Wang, Self-powered electrochemical system by combining Fenton reaction and active chlorine generation for organic contaminant treatment, *Nano Res.* 12 (2019) 2729–2735.
- [15] J. Zhao, G. Zhen, G. Liu, T. Bu, W. Liu, X. Fu, P. Zhang, C. Zhang, Z.L. Wang, Remarkable merits of triboelectric nanogenerator than electromagnetic generator for harvesting small-amplitude mechanical energy, *Nano Energy* 61 (2019) 111–118.
- [16] H. Ouyang, Z. Liu, N. Li, B. Shi, Y. Zou, F. Xie, Y. Ma, Z. Li, H. Li, Q. Zheng, X. Qu, Y. Fan, Z.L. Wang, H. Zhang, Z. Li, Symbiotic cardiac pacemaker, *Nat. Commun.* 10 (2019), 1821.
- [17] Z.L. Wang, Triboelectric nanogenerator (TENG)-sparking an energy and sensor revolution, *Adv. Energy Mater.* 10 (2020), 2000137.
- [18] H. Yang, Y. Pang, T. Bu, W. Liu, J. Luo, D. Jiang, C. Zhang, Z.L. Wang, Triboelectric micromotors actuated by ultralow frequency mechanical stimuli, *Nat. Commun.* 10 (2019), 2309.
- [19] C. Rodrigues, D. Nunes, D. Clemente, N. Mathias, J.M. Correia, P. Rosa-Santos, F. Taveira-Pinto, T. Morais, A.M. Pereira, J. Ventura, Emerging triboelectric nanogenerators for ocean wave energy harvesting: state of the art and future perspectives, *Energy Environ. Sci.* 13 (2020) 2657–2683.
- [20] Z.L. Wang, Catch wave power in floating nets, *Nature* 542 (2017) 159–160.
- [21] X. Liang, T. Jiang, G. Liu, Y. Feng, C. Zhang, Z.L. Wang, Spherical triboelectric nanogenerator integrated with power management module for harvesting multidirectional water wave energy, *Energy Environ. Sci.* 13 (2020) 277–285.
- [22] H. Guo, Z. Wen, Y. Zi, M.-H. Yeh, J. Wang, L. Zhu, C. Hu, Z.L. Wang, A water-proof triboelectric–electromagnetic hybrid generator for energy harvesting in harsh environments, *Adv. Energy Mater.* 6 (2016), 1501593.
- [23] Y. Bai, L. Xu, S. Lin, J. Luo, H. Qin, K. Han, Z.L. Wang, Charge pumping strategy for rotation and sliding type triboelectric nanogenerators, *Adv. Energy Mater.* 10 (2020), 2000605.
- [24] W. Liu, Z. Wang, G. Wang, G. Liu, J. Chen, X. Pu, Y. Xi, X. Wang, H. Guo, C. Hu, Z. L. Wang, Integrated charge excitation triboelectric nanogenerator, *Nat. Commun.* 10 (2019), 1426.
- [25] L. Xu, H. Wu, G. Yao, L. Chen, X. Yang, B. Chen, X. Huang, W. Zhong, X. Chen, Z. Yin, Z.L. Wang, Giant voltage enhancement via triboelectric charge supplement channel for self-powered electroadhesion, *ACS Nano* 12 (2018) 10262–10271.
- [26] L. Xu, T.Z. Bu, X.D. Yang, C. Zhang, Z.L. Wang, Ultrahigh charge density realized by charge pumping at ambient conditions for triboelectric nanogenerators, *Nano Energy* 49 (2018) 625–633.
- [27] F.-R. Fan, L. Lin, G. Zhu, W. Wu, R. Zhang, Z.L. Wang, Transparent triboelectric nanogenerators and self-powered pressure sensors based on micropatterned plastic films, *Nano Lett.* 12 (2012) 3109–3114.
- [28] B. Kim, J. Chung, H. Moon, D. Kim, S. Lee, Elastic spiral triboelectric nanogenerator as a self-charging case for portable electronics, *Nano Energy* 50 (2018) 133–139.
- [29] Y. Pang, S. Chen, Y. Chu, Z.L. Wang, C. Cao, Matryoshka-inspired hierarchically structured triboelectric nanogenerators for wave energy harvesting, *Nano Energy* 66 (2019), 104131.
- [30] P. Rui, W. Zhang, Y. Zhong, X. Wei, Y. Guo, S. Shi, Y. Liao, J. Cheng, P. Wang, High-performance cylindrical pendulum shaped triboelectric nanogenerators driven by water wave energy for full-automatic and self-powered wireless hydrological monitoring system, *Nano Energy* 74 (2020), 104937.
- [31] X. Wang, Z. Wen, H. Guo, C. Wu, X. He, L. Lin, X. Cao, Z.L. Wang, Fully packaged blue energy harvester by hybridizing a rolling triboelectric nanogenerator and an electromagnetic generator, *ACS Nano* 10 (2016) 11369–11376.
- [32] G. Liu, L. Xiao, C. Chen, W. Liu, X. Pu, Z. Wu, C. Hu, Z.L. Wang, Power cables for triboelectric nanogenerator networks for large-scale blue energy harvesting, *Nano Energy* 75 (2020), 104975.
- [33] X. Yang, L. Xu, P. Lin, W. Zhong, Y. Bai, J. Luo, J. Chen, Z.L. Wang, Macroscopic self-assembly network of encapsulated high-performance triboelectric nanogenerators for water wave energy harvesting, *Nano Energy* 60 (2019) 404–412.
- [34] L. Liu, Q. Shi, J.S. Ho, C. Lee, Study of thin film blue energy harvester based on triboelectric nanogenerator and seashore IoT applications, *Nano Energy* 66 (2019), 104167.
- [35] W. Zhong, L. Xu, H. Wang, J. An, Z.L. Wang, Tilting-sensitive triboelectric nanogenerators for energy harvesting from unstable/fluctuating surfaces, *Adv. Funct. Mater.* 29 (2019), 1905319.
- [36] T. Aderinto, H. Li, Ocean wave energy converters: status and challenges, *Energies* 11 (2018) 1250.
- [37] H. Shao, Z. Wen, P. Cheng, N. Sun, Q. Shen, C. Zhou, M. Peng, Y. Yang, X. Xie, X. Sun, Multifunctional power unit by hybridizing contact-separate triboelectric nanogenerator, electromagnetic generator and solar cell for harvesting blue energy, *Nano Energy* 39 (2017) 608–615.
- [38] J. Chen, H. Guo, C. Hu, Z.L. Wang, Robust triboelectric nanogenerator achieved by centrifugal force induced automatic working mode transition, *Adv. Energy Mater.* 10 (2020), 2000886.

- [39] H. Zou, Y. Zhang, L. Guo, P. Wang, X. He, G. Dai, H. Zheng, C. Chen, A.C. Wang, C. Xu, Z.L. Wang, Quantifying the triboelectric series, *Nat. Commun.* 10 (2019), 1427.
- [40] Z.L. Wang, A.C. Wang, On the origin of contact-electrification, *Mater. Today* 30 (2019) 34–51.
- [41] C. Xu, Y. Zi, A.C. Wang, H. Zou, Y. Dai, X. He, P. Wang, Y.C. Wang, P. Feng, D. Li, Z. L. Wang, On the electron-transfer mechanism in the contact-electrification effect, *Adv. Mater.* 30 (2018), 1706790.
- [42] M. Willatzen, Z.L. Wang, Quantum-mechanical model for optical transitions between solids, *Nano Energy* 61 (2019) 311–317.
- [43] G. Xu, X. Li, X. Xia, J. Fu, W. Ding, Y. Zi, On the force and energy conversion in triboelectric nanogenerators, *Nano Energy* 59 (2019) 154–161.
- [44] Z. Lin, B. Zhang, H. Guo, Z. Wu, H. Zou, J. Yang, Z.L. Wang, Super-robust and frequency-multiplied triboelectric nanogenerator for efficient harvesting water and wind energy, *Nano Energy* 64 (2019), 103908.
- [45] Y. Feng, H. Pang, J. An, P. Lu, Y. Feng, X. Liang, W. Zhong, Z.L. Wang, Robust swing-structured triboelectric nanogenerator for efficient blue energy harvesting, *Adv. Energy Mater.* 10 (2020), 2000064.
- [46] Y. Feng, T. Jiang, X. Liang, J. An, Z.L. Wang, Cylindrical triboelectric nanogenerator based on swing structure for efficient harvesting of ultra-low-frequency water wave energy, *Appl. Phys. Rev.* 7 (2020), 021401.
- [47] H. Shao, P. Cheng, R. Chen, L. Xie, N. Sun, Q. Shen, X. Chen, Q. Zhu, Y. Zhang, Y. Liu, Z. Wen, X. Sun, Triboelectric–electromagnetic hybrid generator for harvesting blue energy, *Nano-Micro Lett.* 10 (2018), 54.
- [48] Z. Wen, H. Guo, Y. Zi, M.-H. Yeh, X. Wang, J. Deng, J. Wang, S. Li, C. Hu, L. Zhu, Z. L. Wang, Harvesting broad frequency band blue energy by a triboelectric–electromagnetic hybrid nanogenerator, *ACS Nano* 10 (2016) 6526–6534.



Jie An received his B.S. degree in Maritime Engineering from Dalian Maritime University in 2017. Now he is pursuing his Ph. D. degree in the Beijing Institute of Nanoenergy and Nanosystems, Chinese Academy of Sciences. His research interests are mainly focused on clean energy harvesting and self-powered sensing systems based on triboelectric nanogenerators.



Dr. Tao Jiang is a professor in the Beijing Institute of Nanoenergy and Nanosystems, Chinese Academy of Sciences. He received his B.S. and Ph.D. degrees from School of Materials Science and Engineering, in 2008 and 2014, respectively, from East China University of Science and Technology. After graduation, he worked in the Beijing Institute of Nanoenergy and Nanosystems as a postdoctoral research fellow. His research interests are the theoretical studies of triboelectric nanogenerators, and practical applications in blue energy harvesting.



Yawei Feng received his master degree in Industrial Catalysis from Shanghai Normal University in 2018, and he is currently pursuing his Ph.D. degree in the Beijing Institute of Nanoenergy and Nanosystems, Chinese Academy of Sciences. His research interests are focused on the nanogenerator, self-powered chemistry and the coupling of piezotronics/piezophotonics and catalysis.



Prof. Zhong Lin Wang received his Ph.D. degree from Arizona State University in physics. He now is the Hightower Chair in Materials Science and Engineering, Regents' Professor at Georgia Tech, the chief scientist and director of the Beijing Institute of Nanoenergy and Nanosystems, Chinese Academy of Sciences. Prof. Wang has made original and innovative contributions to the synthesis, discovery, characterization and understanding of fundamental physical properties of oxide nanobelts and nanowires, as well as applications of nanowires in energy sciences, electronics, optoelectronics and biological science. His discovery and breakthroughs in developing nanogenerators establish the principle and technological road map for harvesting mechanical energy from environmental and biological systems for powering personal electronics. His research on self-powered nanosystems has inspired the worldwide efforts in academia and industry for studying energy for micro-nano-systems, which is now a distinct disciplinary in energy research and future sensor networks. He coined and pioneered the fields of piezotronics and piezophotonics by introducing piezoelectric potential gated charge transport process in fabricating new electronic and optoelectronic devices.



Xi Liang received her B.S. degree in Material Science and Engineering from China University of Geosciences in 2016. Now she is a Ph.D. candidate in the Beijing Institute of Nanoenergy and Nanosystems, Chinese Academy of Sciences. Her research interests are focused on blue energy harvesting and self-powered systems.